We consider that the observed high olefin selectivity may largely be due to the stabilization of the propyl radical by the nitroxyl radical site. Indeed, the one-dimensional (1D) nature of this edge avoids the creation of a highly reactive propyl radical (typical of 0D single-site catalysts) (*34*), and also the overoxidation of the adsorbed species (typical of 2D surface catalysts) is suppressed (*35*). The proposed intermediate structures and energies of the overall catalytic cycle are included in fig. S11. We envision that a second abstraction of a hydrogen atom from a primary carbon follows another radical rebound, and creates a di-propoxyl intermediate. Desorption of propene and the reorganization of hydrogen atoms along the edge form water as a side product. The desorption of water is followed by oxygen addition to regenerate the >B–O–O–N< active site. Similar surface reorganization of hydroxyl groups in the presence of oxygen was proposed for related carbon nanofilament catalysts for oxidative dehydrogenation of ethylbenzene to form styrene (*36*). All steps in this process, except for desorption of propene, are exothermic. The second-order rate dependence with respect to $P_{C_3H_8}$ suggests that two propane molecules are required to generate two molecules of water, in line with the overall stoichiometry of the reaction. The desorption of these water molecules forms BN edge vacancies that allow for unique O_2 activation, which explains the influence that the surface coverage of adsorbed oxygen has on the rate of propane consumption.

REFERENCES AND NOTES

1. F. Cavani, J. H. Teles, *ChemSusChem* **2**, 508–534 (2009).
2. J. J. H. B. Sattler, J. Ruiz-Martinez, E. Santillan-Jimenez, B. M. Weckhuysen, *Chem. Rev.* **114**, 10613–10653 (2014).
3. T. Degnan, *Focus Catal.* **2**, 1 (2016).
4. E. G. Rightor, C. L. Tway, *Catal. Today* **258**, 226–229 (2015).
5. T. Ren, M. Patel, K. Blok, *Energy* **31**, 425–451 (2006).
6. K. Chen, A. T. Bell, E. Iglesia, *J. Phys. Chem. B* **104**, 1292–1299 (2000).
7. Z. Wu, H. S. Kim, P. C. Stair, S. Rugmini, S. D. Jackson, *J. Phys. Chem. B* **109**, 2793–2800 (2005).
8. C. A. Carrero, R. Schloegl, I. E. Wachs, R. Schomaecker, *ACS Catal.* **4**, 3357–3380 (2014).
9. D. R. Dreyer, H. P. Jia, C. W. Bielawski, *Angew. Chem. Int. Ed.* **49**, 6813–6816 (2010).
10. J. Zhang *et al.*, *Science* **322**, 73–77 (2008).
11. B. Frank, J. Zhang, R. Blume, R. Schlögl, D. S. Su, *Angew. Chem. Int. Ed. Engl.* **48**, 6913–6917 (2009).
12. J. T. Grant, C. A. Carrero, A. M. Love, R. Verel, I. Hermans, *ACS Catal.* **5**, 5787–5793 (2015).
13. B. Frank, A. Dinse, O. Ovsitser, E. V. Kondratenko, R. Schomäcker, *Appl. Catal. A Gen.* **323**, 66–76 (2007).
14. A. Christodoulakis, M. Machli, A. A. Lemonidou, S. Boghosian, *J. Catal.* **222**, 293–306 (2004).
15. C. Carrero *et al.*, *Catal. Sci. Technol.* **4**, 786–794 (2014).
16. E. V. Kondratenko *et al.*, *J. Catal.* **234**, 131–142 (2005).
17. X. Sun, Y. Ding, B. Zhang, R. Huang, D. S. Su, *Chem. Commun.* (Cambridge) **51**, 9145–9148 (2015).
18. L. Leveles, S. Fuchs, K. Seshan, J. A. Lercher, L. Lefferts, *Appl. Catal. A Gen.* **227**, 287–297 (2002).
19. C. Trionfetti, I. V. Babich, K. Seshan, L. Lefferts, *Appl. Catal. A Gen.* **310**, 105–113 (2006).
20. J. Kibsgaard, Z. Chen, B. N. Reinecke, T. F. Jaramillo, *Nat. Mater.* **11**, 963–969 (2012).
21. F. Cavani, N. Ballarini, A. Cericola, *Catal. Today* **127**, 113–131 (2007).
22. K. Chen, A. Khodakov, J. Yang, A. T. Bell, E. Iglesia, *J. Catal.* **186**, 325–333 (1999).
23. Z. Liu *et al.*, *Nat. Commun.* **4**, 2541 (2013).
24. Y. Chen, J. Zou, S. J. Campbell, G. L. Caer, *Appl. Phys. Lett.* **84**, 2430–2432 (2004).
25. Y. Lin, J. W. Connell, *Nanoscale* **4**, 6908–6939 (2012).
26. N. G. Chopra *et al.*, *Science* **269**, 966–967 (1995).
27. A. Pakdel, Y. Bando, D. Golberg, *Chem. Soc. Rev.* **43**, 934–959 (2014).
28. A. Lopez-Bezanilla, J. Huang, H. Terrones, B. G. Sumpter, *J. Phys. Chem. C* **116**, 15675–15681 (2012).
29. T. Sainsbury *et al.*, *J. Am. Chem. Soc.* **134**, 18758–18771 (2012).
30. P. Nautiyal *et al.*, *Sci. Rep.* **6**, 29498 (2016).
31. G. Kresse, J. Hafner, *Phys. Rev. B* **47**, 558–561 (1993).
32. G. Kresse, D. Joubert, *Phys. Rev. B* **59**, 1758–1775 (1999).
33. N. Turrà, U. Neuenschwander, I. Hermans, *ChemPhysChem* **14**, 1666–1669 (2013).
34. X. Rozanska, R. Fortrie, J. Sauer, *J. Phys. Chem. C* **111**, 6041–6050 (2007).
35. L. C. Grabow, M. Mavrikakis, *ACS Catal.* **1**, 365–384 (2011).
36. G. Mestl, N. I. Maksimova, N. Keller, V. V. Roddatis, R. Schlögl, *Angew. Chem. Int. Ed. Engl.* **40**, 2066–2068 (2001).

ACKNOWLEDGMENTS

We thank the Wisconsin Alumni Research Foundation (WARF) for funding through the WARF Accelerator Program. We thank S. Stahl and J. Dumesic for their helpful feedback when reviewing this manuscript. J.T.G., C.A.C, J.V., A.C., and I.H. are inventors on patent application U.S. 15/260,649, submitted by the WARF, that covers BN as catalysts for ODHP and other related reactions. All data are reported in the main paper and supplementary materials.

SUPPLEMENTARY MATERIALS

www.sciencemag.org/content/354/6319/1570/suppl/DC1
Materials and Methods
Supplementary Text
Figs. S1 to S14
Tables S1 and S2
Movies S1 and S2
References (*37*–*40*)

29 June 2016; resubmitted 26 September 2016
Accepted 16 November 2016
Published online 1 December 2016
10.1126/science.aaf7885

QUANTUM ELECTRONICS

Suppressing relaxation in superconducting qubits by quasiparticle pumping

Simon Gustavsson,[1]* Fei Yan,[1] Gianluigi Catelani,[2] Jonas Bylander,[3] Archana Kamal,[1] Jeffrey Birenbaum,[4] David Hover,[4] Danna Rosenberg,[4] Gabriel Samach,[4] Adam P. Sears,[4] Steven J. Weber,[4] Jonilyn L. Yoder,[4] John Clarke,[5] Andrew J. Kerman,[4] Fumiki Yoshihara,[6] Yasunobu Nakamura,[7,8] Terry P. Orlando,[1] William D. Oliver[1,4,9]

Dynamical error suppression techniques are commonly used to improve coherence in quantum systems. They reduce dephasing errors by applying control pulses designed to reverse erroneous coherent evolution driven by environmental noise. However, such methods cannot correct for irreversible processes such as energy relaxation. We investigate a complementary, stochastic approach to reducing errors: Instead of deterministically reversing the unwanted qubit evolution, we use control pulses to shape the noise environment dynamically. In the context of superconducting qubits, we implement a pumping sequence to reduce the number of unpaired electrons (quasiparticles) in close proximity to the device. A 70% reduction in the quasiparticle density results in a threefold enhancement in qubit relaxation times and a comparable reduction in coherence variability.

Since Hahn's invention of the spin echo in 1950 (*1*), coherent control techniques have been crucial tools for reducing errors, improving control fidelity, performing noise spectroscopy, and generally extending coherence in both natural and artificial spin systems. All of these methods are similar: They correct for dephasing errors by reversing unintended phase accumulations due to a noisy environment through the application of a sequence of control pulses, thereby improving the dephasing time T_2. However, such coherent control techniques cannot correct for irreversible processes that reduce the relaxation time T_1, where energy is lost to the environment. Improving T_1 requires reducing the coupling between the spin system and its noisy environment, reducing the noise in the environment itself (*2*), or implementing full quantum error correction. We demonstrate a pumping sequence that dynamically reduces the noise in the environment and improves T_1 of a superconducting qubit through an irreversible

[1]Research Laboratory of Electronics, Massachusetts Institute of Technology, Cambridge, MA 02139, USA. [2]Forschungszentrum Jülich, Peter Grünberg Institut (PGI-2), 52425 Jülich, Germany. [3]Microtechnology and Nanoscience, Chalmers University of Technology, SE-41296 Gothenburg, Sweden. [4]Massachusetts Institute of Technology (MIT) Lincoln Laboratory, 244 Wood Street, Lexington, MA 02420, USA. [5]Department of Physics, University of California, Berkeley, CA 94720, USA. [6]The Institute of Physical and Chemical Research (RIKEN), Wako, Saitama 351-0198, Japan. [7]Center for Emergent Matter Science (CEMS), RIKEN, Wako, Saitama 351-0198, Japan. [8]Research Center for Advanced Science and Technology (RCAST), The University of Tokyo, Komaba, Meguro-ku, Tokyo 153-8904, Japan. [9]Department of Physics, Massachusetts Institute of Technology, Cambridge, MA 02139, USA.
*Corresponding author. Email: simongus@mit.edu

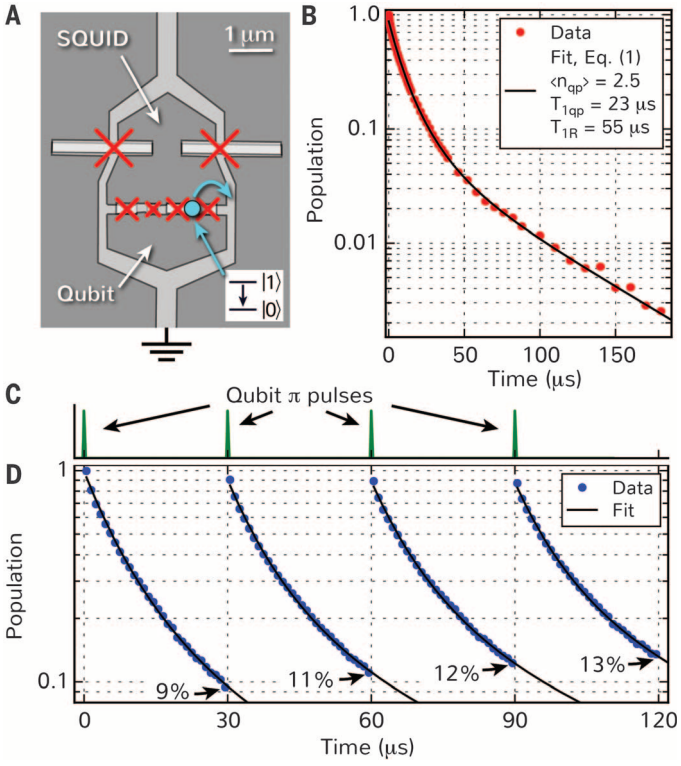

Fig. 1. Nonexponential decay in a superconducting flux qubit. (**A**) Schematic drawing of device A, consisting of a flux qubit (lower loop) coupled to a dc superconducting quantum interference device (SQUID) for qubit readout (outer loop). Red crosses mark the position of the Josephson junctions. Qubit relaxation is induced by quasiparticles tunneling across the qubit junctions, as illustrated by the blue circle. (**B**) Qubit decay, as measured by applying a π pulse and delaying the qubit readout. The decay is clearly nonexponential, with the solid line showing a fit to the decay function expected from quasiparticle tunneling [Eq. 1 in the main text]. (**C**) Pulse sequence for pumping quasiparticles away from the qubit junctions, consisting of multiple qubit π pulses separated by a fixed period ΔT. (**D**) Average qubit population during the pumping sequence, measured by repeating the experiment over 40,000 trials. The remaining population after each pulse interval steadily increases, demonstrating that the qubit decay becomes progressively slower. The solid lines are fits to Eq. 1, with $\langle n_{qp} \rangle$ decreasing as {2.4,1.9,1.7,1.6} from the first to the last decay.

pumping process. The sequence contains the same type of control pulses common to all dynamical-decoupling sequences, but rather than coherently and deterministically controlling the qubit time evolution, the sequence is designed to shape the noise stochastically via inelastic energy exchange with the environment. Similar methods have been used to extend T_2 of spin qubits by dynamic nuclear polarization (*3*), and irreversible control techniques are commonly used to prepare systems into well-defined quantum states through optical pumping (*4*, *5*) and sideband cooling (*6*). However, outside of quantum error correction, to our knowledge no dynamic enhancement of T_1 has been previously reported.

We implement the pumping sequence in a superconducting flux qubit, with the aim of reducing the population of unpaired electrons or quasiparticles in close vicinity to the device. When a superconducting circuit is cooled well below its critical temperature, the quasiparticle density via Bardeen-Cooper-Schrieffer theory is expected to be exponentially suppressed, but a number of experimental groups have reported higher-than-expected values in a wide variety of systems (*7*–*10*). Although the reasons for the enhanced quasiparticle population and the mechanism behind quasiparticle generation are not fully understood, their presence has a number of adverse effects on the qubit performance, causing relaxation (*11*–*16*), dephasing (*17*–*19*), excess excited-state population (*20*), and temporal variations in qubit parameters (*21*–*24*). Moreover, quasiparticles are predicted to be a major obstacle for realizing Majorana qubits in semiconductor nanowires (*25*). Our results provide an in situ technique for removing quasiparticles, especially in conjunction with recent experiments showing that vortices in superconducting electrodes can act as quasiparticles traps, thus keeping the quasiparticles away from the Josephson junctions where they may contribute to qubit relaxation (*22*, *26*–*28*).

We characterize and quantify the quasiparticle population by measuring qubit relaxation. Generally, the relaxation rate is given by a sum of contributions from many different decay channels. Quasiparticles contribute to the relaxation in a process whereby the qubit releases its energy to a quasiparticle tunneling across one of the Josephson junctions (Fig. 1A). Because of the small number of quasiparticles typically present in the device, fluctuations in the quasiparticle population lead to large temporal variations in the qubit decay rate. As a consequence, if the number of quasiparticles changes between trials while one repeats an experiment to determine the average qubit polarization, the time-domain decay no longer behaves as a single exponential but rather takes the following form (*21*) [see also (*29*), section S2]

$$p(t) = e^{\langle n_{qp} \rangle (\exp[-t/\tilde{T}_{1qp}]-1)} e^{-t/T_{1R}} \quad (1)$$

Here, $\langle n_{qp} \rangle$ is the average quasiparticle population in the qubit region during the experiment; t is the time after qubit excitation; $\tilde{T}_{1qp}$ is the relaxation time induced by one quasiparticle; and T_{1R} is the residual relaxation time from other decay channels such as flux noise, Purcell decay, or dielectric losses. Because only quasiparticles are responsible for the nonexponential decay, Eq. 1 provides a direct method for separating out quasiparticle contributions from other relaxation channels.

The experiments are performed using two different flux qubits. Device A is a traditional flux qubit with switching-current readout using a dc superconducting quantum interference device (SQUID), whereas device B is a capacitively shunted (C-shunt) flux qubit (*24*). Qubit A was operated at a frequency of 5.4 GHz, whereas qubit B was operated at 4.7 GHz [for more information on qubit parameters, see sections S1 and S6 in (*29*)]. Figure 1B shows the measured relaxation of qubit A, together with a fit to Eq. 1. The decay is clearly nonexponential: The fast initial decay due to quasiparticle fluctuations is followed by a slower, constant decay attributable to residual relaxation channels. From the fit, we find an average quasiparticle population $\langle n_{qp} \rangle = 2.5$, with $\tilde{T}_{1qp} = 23$ μs and $T_{1R} = 55$ μs. We have also measured the qubit decay as a function of flux and temperature to further validate its sensitivity to quasiparticles [sections S3 and S4 in (*29*)].

The same mechanism that leads to qubit relaxation also provides an opportunity for reducing the quasiparticle population. When the qubit relaxes through a quasiparticle tunneling event, the quasiparticle both tunnels to a different island and acquires an energy $\hbar\omega_0$ from the qubit ($\omega_0/2\pi$ is the qubit frequency and $\hbar$ is Planck's constant h divided by 2π). The increase in energy leads to a higher quasiparticle velocity (at a constant mean free path) so that a quasiparticle can move more quickly away from the regions close to the qubit junctions where it may cause qubit relaxation. The situation is depicted in Fig. 1A, where the quasiparticle tunneling out from the section of the qubit loop containing the junctions may diffuse away toward the normal-metal ground electrode. We make use of this mechanism by applying a pulse sequence (Fig. 1C) consisting of several qubit π pulses separated by a fixed period (in this case, $\Delta T = 30$ μs). The first π pulse excites the qubit into state $|1\rangle$ and, during the subsequent waiting time, it has some probability of relaxing to the ground state. Because $\tilde{T}_{1qp} < T_{1R}$, this most likely occurs through a quasiparticle tunneling event, which transfers a quasiparticle across a junction, increases the quasiparticle energy, and thereby enhances its diffusion rate. The process is stochastic and may transfer quasiparticle in any direction, but by repeating the sequence we expect to pump

quasiparticles away from the qubit junctions. The measured average qubit polarization during the pumping sequence (Fig. 1D) starts with the qubit in the ground state, the first π pulse brings the qubit to $|1\rangle$, and during the following waiting period the qubit relaxes back to an average polarization of 9%. The second π pulse inverts the polarization to 91%, and the qubit starts decaying again. However, at the end of the second waiting period the remaining polarization is 11%, demonstrating that the decay is slower during the second interval. The third and fourth π pulses further retard the decay, yielding a remaining polarization of 12 and 13%, respectively. Note that the excess population can be removed by using single-shot readout techniques to reset the qubit state after the pumping sequence ends (*30*).

We quantify the reduction in qubit decay by extending the pump sequence to contain more π pulses and fitting the decay to Eq. 1. The measured qubit decay, using up to 40 pumping pulses (Fig. 2), demonstrates a more than threefold enhancement in qubit decay time compared with the bare decay (the decay time is defined as the time $T_{1/e}$ it takes for the signal to decay by a factor of $1/e$). The solid lines in Fig. 2B are fits to Eq. 1; Fig. 2, C and D, show the resulting fitting parameters $\langle n_{qp}\rangle$ and $\tilde{T}_{1qp}$ as a function of the number of pumping pulses. The average quasiparticle population drops from $\langle n_{qp}\rangle = 2.2$ to $\langle n_{qp}\rangle \sim 0.5$ after 40 pulses and then saturates at this level. Simultaneously, the decay time associated with one quasiparticle drops from $\tilde{T}_{1qp} = 20\,\mu s$ to $\tilde{T}_{1qp} \sim 7\,\mu s$. The reduction of $\tilde{T}_{1qp}$ is somewhat surprising, as one might generally expect the decay time per quasiparticle to remain constant as the quasiparticles are pumped away. However, as the number of π pulses increases, the quasiparticles remaining near the junctions generally have higher energy and, hence, cause qubit excitation as well as qubit relaxation. Because $1/\tilde{T}_{1qp}$ is the sum of decay and excitation rates, this conceptually explains, at least in part, the suppression of $\tilde{T}_{1qp}$. Note that despite the introduction of an excitation rate, the qubit will still eventually decay to $|0\rangle$ due to non-quasiparticle relaxation channels (T_{1R}), preventing us from determining the excitation and decay rate separately from the steady-state qubit population. Additionally, the range of values of $\tilde{T}_{1qp}$ reported here is consistent with previous measurements in flux qubits (*31*).

To further validate the quasiparticle pumping model and rule out alternate explanations of the data, we have also implemented the same pumping scheme, using pulses corresponding to 2π instead of π rotations. If the qubit's environment were directly influenced by the microwave pulses through a mechanism other than quasiparticle pumping (e.g., heating, or saturation of two-level systems), we would expect both the π and 2π pulses to affect the qubit decay time. However, in the experiment we only observe an improvement in the qubit decay when driving the system with π pulses, consistent with the quasiparticle pumping model [(*29*), section S7].

Having demonstrated that the pumping sequence can substantially reduce the quasiparticle population, we introduced a variable delay before the final probe pulse to investigate how long the reduction in $\langle n_{qp}\rangle$ persists before it returns to the equilibrium value [see (*29*), section S5]. With the exception of an initial, faster rate for $t_{delay} < 50\,\mu s$, the return to its steady state is well described by an exponential function with a time constant of 300 μs. The time scale for quasiparticle recovery is much longer than the qubit lifetime, thus justifying the use of the steady-state solution in Eq. 1 for estimating the quasiparticle population.

The measured quasiparticle population range of $\langle n_{qp}\rangle \sim 0.5$ to 2.5 corresponds to an upper bound on the normalized quasiparticle density of $\chi_{qp} \sim 10^{-4}$ to 10^{-5}, where χ_{qp} is the number of quasiparticles divided by the number of Cooper pairs, and we assume that all decay-inducing quasiparticles are confined to the qubit islands. This is higher than the typical values of $\chi_{qp} \sim 10^{-6}$ to 10^{-7} reported in the literature (*7*–*10*). The difference may possibly be attributed to the switching current readout of device A, where the qubit state is inferred by applying a short current pulse to the SQUID and determining its probability to switch to the normal state. Whenever

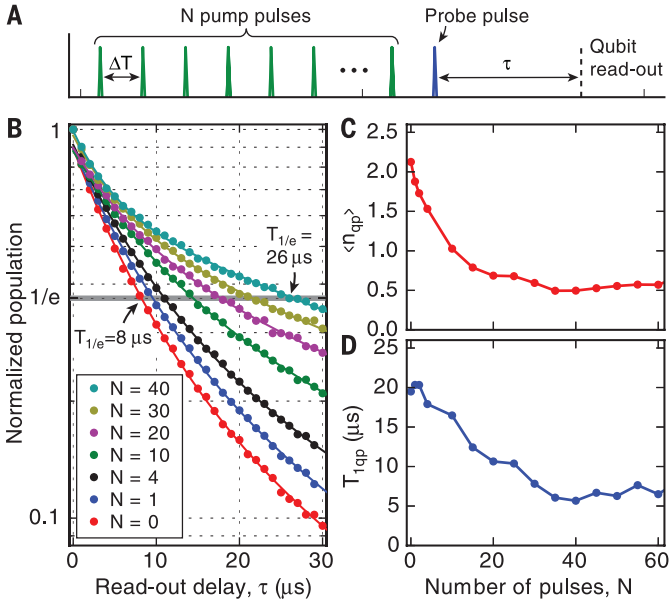

Fig. 2. Dynamic improvement in qubit decay time. (**A**) Pulse sequence for pumping quasiparticles. The last π pulse acts as a probe pulse to measure the qubit polarization. (**B**) Normalized population versus readout delay, showing qubit decay after the pump sequence, measured with $\Delta T = 10\,\mu s$ for an increasing number of pulses N. The decay time steadily increases from $T_{1/e} = 8$ to 26 μs after 40 pump pulses. The decay traces have been normalized to the population at $\tau = 0$ to allow direct comparison. Solid lines are fits to Eq. 1. Each data point is averaged over 10^5 trials. (**C**) Average quasiparticle number $\langle n_{qp}\rangle$ and (**D**) decay rate per quasiparticle $\tilde{T}_{1qp}$, extracted from the fits shown in (B). T_{1R} is held constant at 55 μs for all fits.

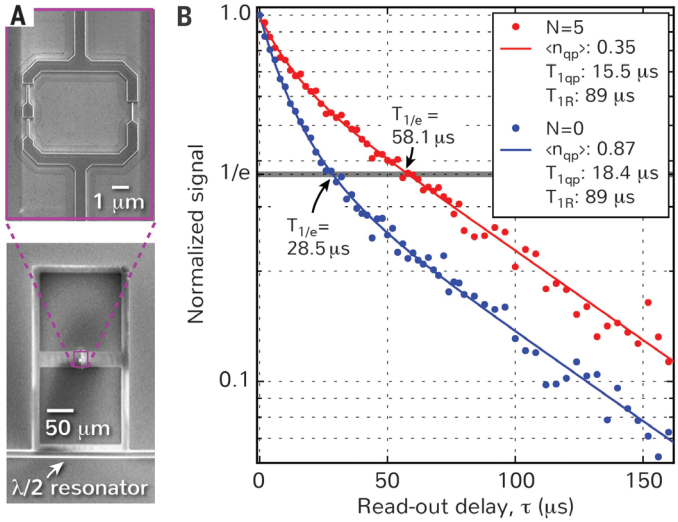

Fig. 3. Improvement in qubit decay time for a C-shunt flux qubit. (**A**) Scanning electron microscopy image of device B, showing the large square capacitor plates (bottom) and a magnification of the qubit loop containing the three Josephson junctions (top). The qubit is coupled to a half-wavelength (λ/2) resonator. (**B**) Qubit relaxation, measured with and without quasiparticle pumping pulses. The trace with $N = 5$ pumping pulses was taken with a pulse period of $\Delta T = 30\,\mu s$. The data are averaged from 15 individual traces, acquired over a 1-hour period. The fit was performed assuming the same value of T_{1R} for both traces. The uncertainties in fitting parameters are $\langle n_{qp}\rangle$: ±0.02, $\tilde{T}_{1qp}$: ±3.5 μs, and T_{1R}: ±4 μs.

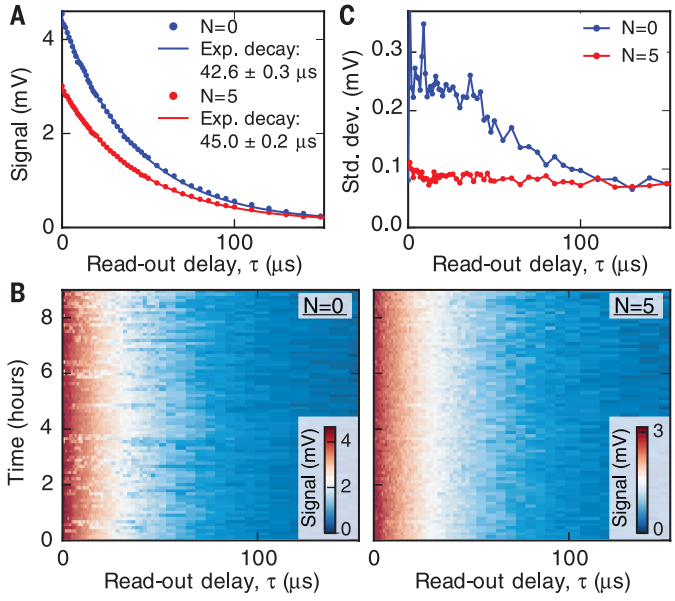

Fig. 4. Reduction of qubit coherence variations with quasiparticle pumping. (**A**) Averaged qubit decay, measured with and without pumping pulses. The decay function is close to exponential in both cases. The decay time increases by ~6% with the pumping pulses. The traces have not been normalized to account for the decay during the pulse sequence, causing reduced contrast for the data with $N = 5$. The data were measured with $\Delta T = 30$ μs. (**B**) Individual traces of the averaged decay data shown in (A), measured without (left) and with five pumping pulses (right). The pumping sequence substantially reduces the temporal fluctuations observed in the decay without pumping pulses. (**C**) Standard deviation of the data in (B), demonstrating the strong reduction in temporal shot-to-shot fluctuations in the presence of the pumping pulses.

a switching event occurs, quasiparticles are created in close vicinity to the SQUID junctions, leading to an increase in the overall quasiparticle density.

We next investigate quasiparticle pumping in a dispersively read-out C-shunt flux qubit (device B), consisting of a flux qubit loop shunted by a large capacitance (Fig. 3A). Although the capacitor improves the qubit coherence by reducing its sensitivity to charge noise, the C-shunt flux qubit is still affected by quasiparticle fluctuations. As reported in (*24*), the qubit was observed to switch between a stable configuration, with a purely exponential decay with $T_1 > 50$ μs, and an unstable configuration, with nonexponential decay and temporal fluctuations. The switching between the various configurations was found to occur on a slow time scale, ranging from hours to several days. Similar switching events between stable and unstable configurations have also been observed in a fluxonium qubit and were attributed to fluctuations in the quasiparticle density (*22*).

We next investigated how the quasiparticle pumping sequence affects the coherence of device B, both in stable and unstable configurations. Because the switching between different configurations is random but slow, we were careful to average only over intervals when no switching event occurred. Figure 3B shows the decay of device B, measured with and without $N = 5$ quasiparticle pumping pulses. The data were taken when the device was in a configuration where the qubit decay was clearly nonexponential, which is well captured by fits to Eq. 1 (solid lines in Fig. 3B). We observed a drop in the quasiparticle population from 0.87 to 0.35, leading to a twofold enhancement in the qubit decay time. Note that the long-time decay rate is identical for both traces, as expected because the pumping scheme does not affect nonquasiparticle relaxation channels. The results demonstrate that the pumping scheme works even though device B does not have a ground electrode for trapping quasiparticles, but it has been shown that vortices in the capacitor pads can also act as quasiparticle traps (*26*). The pumping scheme should also be applicable to other qubit modalities in which quasiparticle tunneling contributes to qubit relaxation.

The data in Fig. 3B were acquired by continuously measuring qubit decay traces over a 1-hour period and averaging them together. Figure 4 shows similar repeated measurements of the qubit decay with and without pumping pulses, but these traces were acquired about a week after the data in Fig. 3. In the more recent data set, the qubit is in a configuration where the averaged decay function is relatively well described by a single exponential, both with and without pumping pulses (Fig. 4A), and the five pumping pulses improve the decay time by only ~6%. However, when investigating the individual decay traces (Fig. 4B), we found substantial amounts of noise and temporal fluctuations in the readout signal for the data without pumping pulses. These random variations vanish when implementing the pumping sequence (right panel of Fig. 4B).

To quantify the improvements in variability, we calculated the standard deviation of the readout signal over 9 hours of data (Fig. 4C). With pumping pulses, the standard deviation is independent of the readout delay τ and can be ascribed to the noise of the high–electron-mobility (HEMT) amplifier used for amplification. Without pumping pulses, the standard deviation is substantially larger for $\tau < 50$ μs but approaches the same level as for $N = 5$ for long delay times. The increased noise is caused by variations in the qubit T_1 time, which lead to strong fluctuations in the qubit population directly after the initial π pulse. The fluctuations are reduced as the qubit decays to the ground states for long τ, leaving only the contributions from the HEMT noise.

Our implementation of a stochastic scheme to dynamically shape the environment by pumping quasiparticles in a superconducting flux qubit lead to substantial improvements in both qubit coherence times and coherence variability. In addition to applications in superconducting qubits, we anticipate our results to be of practical importance for implementing Majorana fermions in hybrid semiconductor–superconductor systems, where the presence of a single quasiparticle is detrimental to the device performance (*25*).

REFERENCES AND NOTES

1. E. Hahn, *Phys. Rev.* **80**, 580–594 (1950).
2. K. W. Murch, S. J. Weber, K. M. Beck, E. Ginossar, I. Siddiqi, *Nature* **499**, 62–65 (2013).
3. D. J. Reilly *et al.*, *Science* **321**, 817–821 (2008).
4. W. Happer, *Rev. Mod. Phys.* **44**, 169–249 (1972).
5. S. O. Valenzuela *et al.*, *Science* **314**, 1589–1592 (2006).
6. D. Wineland, R. Drullinger, F. Walls, *Phys. Rev. Lett.* **40**, 1639–1642 (1978).
7. J. Aumentado, M. W. Keller, J. M. Martinis, M. H. Devoret, *Phys. Rev. Lett.* **92**, 066802 (2004).
8. P. J. D. Visser *et al.*, *Phys. Rev. Lett.* **106**, 167004 (2011).
9. V. F. Maisi *et al.*, *Phys. Rev. Lett.* **111**, 147001 (2013).
10. E. M. Levenson-Falk, F. Kos, R. Vijay, L. Glazman, I. Siddiqi, *Phys. Rev. Lett.* **112**, 047002 (2014).
11. R. Lutchyn, L. Glazman, A. Larkin, *Phys. Rev. B* **72**, 014517 (2005).
12. J. M. Martinis, M. Ansmann, J. Aumentado, *Phys. Rev. Lett.* **103**, 097002 (2009).
13. G. Catelani *et al.*, *Phys. Rev. Lett.* **106**, 077002 (2011).
14. J. Leppäkangas, M. Marthaler, *Phys. Rev. B* **85**, 144503 (2012).
15. L. Sun *et al.*, *Phys. Rev. Lett.* **108**, 230509 (2012).
16. D. Ristè *et al.*, *Nat. Commun.* **4**, 1913 (2013).
17. J. Schreier *et al.*, *Phys. Rev. B* **77**, 180502 (2008).
18. G. Catelani, S. E. Nigg, S. M. Girvin, R. J. Schoelkopf, L. I. Glazman, *Phys. Rev. B* **86**, 184514 (2012).
19. S. E. de Graaf *et al.*, *Phys. Rev. Lett.* **111**, 137002 (2013).
20. J. Wenner *et al.*, *Phys. Rev. Lett.* **110**, 150502 (2013).
21. I. M. Pop *et al.*, *Nature* **508**, 369–372 (2014).
22. U. Vool *et al.*, *Phys. Rev. Lett.* **113**, 247001 (2014).
23. M. Bal, M. H. Ansari, J.-L. Orgiazzi, R. M. Lutchyn, A. Lupascu, *Phys. Rev. B* **91**, 195434 (2015).
24. F. Yan *et al.*, *Nat. Commun.* **7**, 12964 (2016).
25. D. Rainis, D. Loss, *Phys. Rev. B* **85**, 174533 (2012).
26. C. Wang *et al.*, *Nat. Commun.* **5**, 5836 (2014).
27. I. Nsanzineza, B. L. Plourde, *Phys. Rev. Lett.* **113**, 117002 (2014).
28. M. Taupin, I. M. Khaymovich, M. Meschke, A. S. Mel'nikov, J. P. Pekola, *Nat. Commun.* **7**, 10977 (2016).
29. Supplementary materials are available on *Science* Online.
30. K. Geerlings *et al.*, *Phys. Rev. Lett.* **110**, 120501 (2013).
31. M. Stern *et al.*, *Phys. Rev. Lett.* **113**, 123601 (2014).

ACKNOWLEDGMENTS

We thank M. Blencowe, D. Campbell, M. Devoret, J. Grover, P. Krantz, and I. Pop for useful discussions and P. Baldo, V. Bolkhovsky, G. Fitch, J. Miloshi, P. Murphy, B. Osadchy, K. Parrillo, R. Slattery, and T. Weir at MIT Lincoln Laboratory for technical assistance. This research was funded in part by the Office of the Director of National Intelligence (ODNI), Intelligence Advanced Research Projects Activity (IARPA), and the Assistant Secretary of Defense for Research and Engineering via MIT Lincoln Laboratory

under Air Force contract no. FA8721-05-C-0002; by the U.S. Army Research Office grant no. W911NF-14-1-0682; and by NSF grant no. PHY-1415514. The views and conclusions contained herein are those of the authors and should not be interpreted as necessarily representing the official policies or endorsements, either expressed or implied, of ODNI, IARPA, or the U.S. government. G.C. acknowledges partial support by the European Union (EU) under Research Executive Agency (REA) grant agreement no. CIG-618258. J.By. acknowledges partial support by the EU under REA grant agreement no. CIG-618353.

SUPPLEMENTARY MATERIALS

www.sciencemag.org/content/354/6319/1573/suppl/DC1
Supplementary Text
Figs. S1 to S4
References (*32*–*37*)

18 July 2016; accepted 21 November 2016
Published online 8 December 2016
10.1126/science.aah5844

QUANTUM OPTICS

Quantum optical circulator controlled by a single chirally coupled atom

Michael Scheucher, Adèle Hilico, Elisa Will, Jürgen Volz,* Arno Rauschenbeutel*

Integrated nonreciprocal optical components, which have an inherent asymmetry between their forward and backward propagation direction, are key for routing signals in photonic circuits. Here, we demonstrate a fiber-integrated quantum optical circulator operated by a single atom. Its nonreciprocal behavior arises from the chiral interaction between the atom and the transversally confined light. We demonstrate that the internal quantum state of the atom controls the operation direction of the circulator and that it features a strongly nonlinear response at the single-photon level. This enables, for example, photon number–dependent routing and novel quantum simulation protocols. Furthermore, such a circulator can in principle be prepared in a coherent superposition of its operational states and may become a key element for quantum information processing in scalable integrated optical circuits.

As their electronic counterparts, integrated optical circuits require nonreciprocal elements, such as diodes and circulators, for signal routing and processing. Bulk optical implementations of such components are readily available and rely mostly on a nonreciprocal polarization rotation via the Faraday effect. However, this mechanism cannot straightforwardly be translated to integrated optics because nanooptical structures are typically birefringent (*1*). Demonstrations of integrated nonreciprocal devices therefore rather used, for example, nonlinear optical effects (*2*–*4*), time-modulation of the waveguide (*5*–*7*), or magneto-optical effects in conjunction with the extraordinary polarization properties of strongly confined light fields (*1*, *8*, *9*). None of these approaches could simultaneously realize strong nonreciprocity, low loss, and compatibility with low light levels. However, these characteristics are crucial when it comes to quantum applications such as quantum communication (*10*), quantum information processing (*11*), and quantum simulation (*12*). There, information is encoded in individual photons, and their loss must be avoided as much as possible. This condition narrows down the scope of quantum-compatible nonreciprocal optical elements to nonreciprocal phase shifters and circulators.

We experimentally realized a fiber-integrated circulator that is capable of routing individual photons for quantum optical applications. It is operated by a single atom that is coupled to the evanescent field of a whispering-gallery-mode (WGM) microresonator. The latter is interfaced with two coupling fibers (*13*, *14*), realizing a four-port device (Fig. 1A). We demonstrate that the internal quantum state of the atom controls the operation direction of the circulator. Furthermore, we show that being controlled by a single atom, our device features photon number–dependent routing capability that has application in, for example, novel quantum simulation protocols.

In order to achieve efficient routing, the coupling rates κ_a and κ_b between the resonator field and the field in the respective coupling fiber "a" or "b" are adjusted so that both fibers are approximately critically coupled to the empty resonator: $\kappa_a \approx \kappa_b \gg \kappa_0$, where κ_0 is the intrinsic resonator field decay rate. When no atom is coupled to the resonator mode, this realizes an add-drop filter (*13*, *14*) in which light that is launched into one fiber will be transferred to the other fiber via the resonator. Because of its strong transverse confinement, the evanescent field of the clockwise (cw) propagating resonator mode is almost fully circularly polarized (*15*). Its electric field vector rotates counterclockwise in the plane orthogonal to the resonator axis (z axis), corresponding to σ^- polarization (Fig. 1B). Time-reversal symmetry then implies that the evanescent field of the counterclockwise (ccw) propagating mode is almost fully σ^+-polarized (*15*). Coupling such "spin orbit–locked" light fields to single quantum emitters gives rise to the new paradigm of chiral quantum optics (*16*). In the context of WGMs, it recently enabled the implementation of an optical switch controlled by a single photon (*17*) and the extraction of a single photon from an optical pulse (*18*). Moreover, an optical isolator was realized that either transmits or dissipates fiber-guided light depending on its propagation direction (*19*). For the circulator, we resonantly coupled a single ^{85}Rb atom to the resonator, which is prepared in the outermost Zeeman sublevel $m_F = +3$ of the $5S_{1/2}$, $F = 3$ hyperfine ground state. Thus, the two counter-propagating resonator modes couple to an effective V-level system (Fig. 1C). Remarkably, the strength of the transition to the $5P_{3/2}$, $F' = 4$, $m_{F'} = +4$ excited state is 28 times stronger than that to the $F' = 4$, $m_{F'} = +2$ state (*20*). As a consequence, light in the ccw mode interacts strongly with the atom with a coupling strength g_{ccw}, whereas light in the cw mode exhibits much weaker coupling, $g_{cw} \ll g_{ccw}$. This chiral (direction-dependent) light-matter interaction breaks Lorentz reciprocity (*19*, *21*–*25*). In particular, the presence of the atom changes the resonator field decay rate from $\kappa_{tot} = \kappa_0 + \kappa_a + \kappa_b$ to $\kappa_{tot} + \Gamma_{cw/ccw}$, where $\Gamma_{cw/ccw} = g^2_{cw/ccw}/\gamma$ is the direction-dependent atom-induced loss rate (*26*) and $\gamma = 2\pi \times 3$ MHz is the dipole decay rate of Rb. For light in the cw mode, Γ_{cw} is small, and the field decay rate is not substantially modified by the atom, whereas for the ccw mode, Γ_{ccw} can become comparable with or even exceed κ_{tot}. Consequently, the add-drop functionality is maintained when light is launched into those fiber ports for which it couples to the cw mode (Fig. 1D, input ports 2 and 4). However, for the two other input ports (Fig. 1D, 1 and 3), the light couples to the ccw mode, and the resonator-atom system operates in the undercoupled regime

$$\kappa_a, \kappa_b \ll \Gamma_{ccw} \quad (1)$$

Thus, the incident light field remains in its initial fiber. Overall, the device thus realizes an optical circulator that routes light from the input port i to the adjacent output port $i + 1$ with $i \in \{1, 2, 3, 4\}$ (Fig. 1D). Preparing the atom in the opposite Zeeman ground state, $F = 3$, $m_F = -3$, exchanges the roles of the cw and ccw mode and thus yields a circulator with reversed operation direction. Hence, the circulator is programmable, and its operation direction is defined by the internal state of the atom.

For nonperfect circular polarization of the modes and our experimental parameters ($g_{ccw} \approx 2\pi \times 12$ MHz), the ratio between $\Gamma_{ccw} \approx 2\pi \times 48$ MHz and $\Gamma_{cw} \approx 2\pi \times 1.7$ MHz is finite (*26*). Concerning the performance of the circulator, there is thus a trade-off between efficient light transfer from

Vienna Center for Quantum Science and Technology, Atominstitut, Technischen Universität Wien Stadionallee 2, 1020 Vienna, Austria.
*Corresponding author. Email: jvolz@ati.ac.at (J.V.); arno.rauschenbeutel@ati.ac.at (A.R.)

Suppressing relaxation in superconducting qubits by quasiparticle pumping

Simon Gustavsson, Fei Yan, Gianluigi Catelani, Jonas Bylander, Archana Kamal, Jeffrey Birenbaum, David Hover, Danna Rosenberg, Gabriel Samach, Adam P. Sears, Steven J. Weber, Jonilyn L. Yoder, John Clarke, Andrew J. Kerman, Fumiki Yoshihara, Yasunobu Nakamura, Terry P. Orlando and William D. Oliver (December 8, 2016)

Science **354** (6319), 1573-1577. [doi: 10.1126/science.aah5844] originally published online December 8, 2016

Editor's Summary

Science (print ISSN 0036-8075; online ISSN 1095-9203) is published weekly, except the last week in December, by the American Association for the Advancement of Science, 1200 New York Avenue NW, Washington, DC 20005.